A&A 607, A126 (2017)
DOI: 10.1051/0004-6361/201730987

Astronomy & Astrophysics

The optimally sampled galaxy-wide stellar initial mass function

Observational tests and the publicly available GalIMF code*

Zhiqiang Yan[1], Tereza Jerabkova[2,3], and Pavel Kroupa[2,3]

[1] Argelander-Institut für Astronomie, Universität Bonn, Auf dem Hügel 71, 53121 Bonn, Germany
e-mail: 1832332677@qq.com
[2] Helmholtz-Institut für Strahlen- und Kernphysik (HISKP), Universität Bonn, Nussallee 14–16, 53115 Bonn, Germany
e-mail: pavel@astro.uni-bonn.de
[3] Charles University in Prague, Faculty of Mathematics and Physics, Astronomical Institute, V Holešovičkách 2, 180 00 Praha 8, Czech Republic
e-mail: tereza@sirrah.troja.mff.cuni.cz

Received 13 April 2017 / Accepted 12 July 2017

ABSTRACT

Here we present a full description of the integrated galaxy-wide initial mass function (IGIMF) theory in terms of the optimal sampling and compare it with available observations. Optimal sampling is the method we use to discretize the IMF deterministically into stellar masses. Evidence indicates that nature may be closer to deterministic sampling as observations suggest a smaller scatter of various relevant observables than random sampling would give, which may result from a high level of self-regulation during the star formation process. We document the variation of IGIMFs under various assumptions. The results of the IGIMF theory are consistent with the empirical relation between the total mass of a star cluster and the mass of its most massive star, and the empirical relation between the star formation rate (SFR) of a galaxy and the mass of its most massive cluster. Particularly, we note a natural agreement with the empirical relation between the IMF power-law index and the SFR of a galaxy. The IGIMF also results in a relation between the SFR of a galaxy and the mass of its most massive star such that, if there were no binaries, galaxies with $SFR < 10^{-4}\ M_{\odot}$/yr should host no Type II supernova events. In addition, a specific list of initial stellar masses can be useful in numerical simulations of stellar systems. For the first time, we show optimally sampled galaxy-wide IMFs (OSGIMF) that mimic the IGIMF with an additional serrated feature. Finally, a Python module, GalIMF, is provided allowing the calculation of the IGIMF and OSGIMF dependent on the galaxy-wide SFR and metallicity.

Key words. galaxies: stellar content – galaxies: luminosity function, mass function – galaxies: star formation – galaxies: formation – galaxies: star clusters: general – galaxies: evolution

1. Introduction

The initial distribution of stellar masses as the outcome of star formation is fundamentally important for understanding the evolution of stellar systems on star-cluster and galaxy scales. Much effort has been invested in constraining the shape (Salpeter 1955; Scalo 1986; Kroupa 2001; Chabrier 2003) and possible variation of the stellar initial mass function (IMF; Hopkins 2013). On the star-cluster scale, an invariant IMF has usually been deduced (Kroupa 2001; Bastian et al. 2010; Kroupa et al. 2013), although a variation of the IMF in extreme star-burst clusters has been suggested given observational data (Dabringhausen et al. 2012; Marks et al. 2012; Banerjee & Kroupa 2015). On the galaxy scale, evidence for a variable IMF has been reported (Matteucci & Brocato 1990; Vazdekis et al. 2003; Hoversten & Glazebrook 2008; Meurer et al. 2009; Lee et al. 2009; Gunawardhana et al. 2011). While the theories describing star formation and IMF are neither fully developed nor understood, a successful theory must be consistent with the observations both on star cluster and galaxy scales and also needs to be able to make predictions of new phenomena.

Here we study a particular approach, the integrated galaxy-wide initial mass function (IGIMF) theory, developed for calculating galaxy-wide IMFs but starting with the IMF constrained observationally on star-cluster scales. With this semi-empirical approach, we can constrain the star-cluster-scale IMF and galaxy-wide IMF and potentially understand the variations of the IMF in different stellar systems.

The IGIMF theory was introduced by Kroupa & Weidner (2003) in which it was called the "field-star IMF". This theory was originally based on a universal IMF on the star-cluster scale (with later adoption of a systematically varying IMF; see Axiom 3 below) and an embedded cluster mass function (ECMF)[1] to generate a variable IGIMF on a galactic scale, leading to a good description in explaining observations, for example, most recently, Gargiulo et al. (2015) and

* A copy of the python code model is available at the CDS via anonymous ftp to cdsarc.u-strasbg.fr (130.79.128.5) or via http://cdsarc.u-strasbg.fr/viz-bin/qcat?J/A+A/607/A126

[1] An embedded cluster refers to a correlated star formation event, i.e., a gravitationally driven collective process of transformation of the interstellar gaseous matter into stars in molecular-cloud overdensities on a spatial scale of about one pc and within about one Myr (Lada & Lada 2003; Kroupa et al. 2013; Megeath et al. 2016). The value $M_{\rm ecl}$ is the mass of all stars formed in the embedded cluster.

Fontanot et al. (2017). The theory also made the prediction that dwarf galaxies must show a deficit of Hα emission relative to UV emission; see Pflamm-Altenburg et al. (2007, 2009). This was verified to be the case in Lee et al. (2009).

It is important to know that an additional condition is required to make the IGIMF theory work. That is, one needs to apply a certain sampling method that determines the stellar masses of a stellar system with a given IMF. It has been shown that the IGIMF theory with random unconditional sampling from an IMF is not consistent with observations (e.g., Fumagalli et al. 2011; Andrews et al. 2013; Dib et al. 2017, as further discussed in Appendix A).

Although the shape of the IMF can be estimated by observations to some extent, the sampling procedure that determines the mass of each generated star in a simulation is another issue. Whether it should be random sampling, deterministic sampling, or somewhere in between needs to be clarified.

Evidence collated in Kroupa (2002); Kroupa et al. (2013), have found that the simplest interpretation of the IMF, where the IMF is interpreted as a probability distribution function from which stars are randomly sampled, may fail to reproduce the observations because the observed IMF power-law index above a few $M_\odot$ shows a scatter that is smaller than random sampling would give (see Kroupa et al. 2013, their Fig. 27). Furthermore, Hsu et al. (2012, 2013) have shown that there are star-forming regions with large total stellar mass but a significant deficiency in massive stars; this is inconsistent with a stochastic scenario in which 1000 small star clusters of 100 $M_\odot$ would statistically generate the same stellar population as a single 10^5 $M_\odot$ star cluster.

In addition, the recent studies from Stephens et al. (2017) and others (see Fig. 1 below) have supported a significant empirical correlation of the maximum stellar mass in a cluster and the mass in stars of an embedded cluster (the $m_{\rm str,max}$–$M_{\rm ecl}$ relation). The relation was first indicated by Weidner & Kroupa (2006) and has been further discussed in Weidner et al. (2013a). The authors have argued that the data disagree with the random sampling with a high confidence.

However, there is still a discussion about whether the $m_{\rm str,max}$–$M_{\rm ecl}$ relation is consistent with a randomly sampled invariant IMF. Even though it has been shown by Weidner et al. (2014) that the $m_{\rm str,max}$–$M_{\rm ecl}$ observations disfavor random sampling, we will discuss this issue in more detail in the future. A further study applying two statistical tests (a KS test and standard deviations of the distance between data points) in Yan et al. (in prep.) has shown that the observations disfavor the scenario of random sampling of stellar masses with a confidence of 4σ.

This paper studies a deterministic method called "optimal sampling" introduced by Kroupa et al. (2013). With this method the IMF is populated smoothly with no Poisson noise; this is favored by observations in comparison with random sampling as is demonstrated in Sect. 4.1 below.

One counterargument against the optimal sampling scenario is that high mass stars form only in massive parent clusters according to the optimal sampling. But it appears that about 4% of the O stars are observed in an isolated state. This disagreement has been lifted since Gvaramadze et al. (2012) have shown that most known isolated O stars are ejected stars related to a parent cluster; very few of the O stars that cannot be traced back to their birth cluster are possibly due to the two-step ejection mechanism described by Pflamm-Altenburg & Kroupa (2010). Recently using the *Hubble* Space Telescope, Stephens et al. (2017) have specifically looked at seven massive stars thought previously, from *Spitzer* observations, to be isolated massive stars in the Large Magellanic Cloud. All of these seven stars turn out to be within substantial but compact clusters lying on the $m_{\rm str,max}$–$M_{\rm ecl}$ relation, which supports the conclusion of Gvaramadze et al. (2012) and statistically disfavors the random drawing scenario.

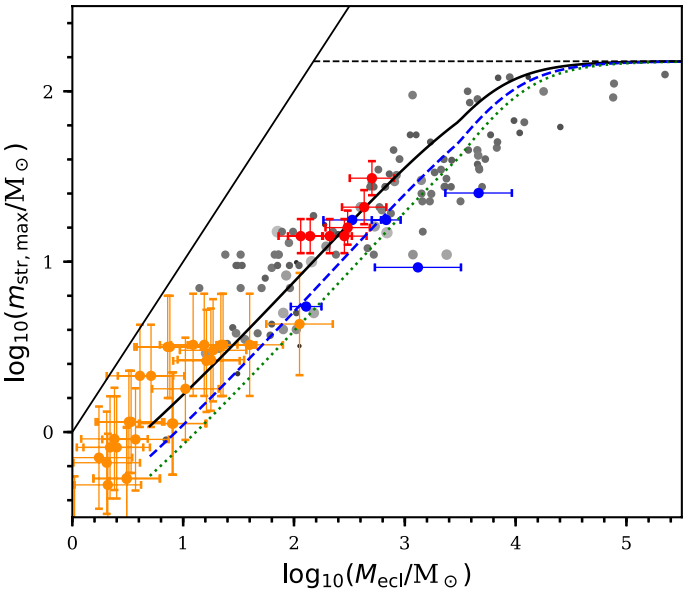

Fig. 1. Most massive stellar mass to embedded cluster mass ($m_{\rm str,max}$–$M_{\rm ecl}$) relation. The optimally sampled results for the most, second, and third massive star mass as a function of embedded cluster mass are shown as a solid curve, blue dashed curve, and green dotted curve, respectively. Observational data come from Kirk & Myers (2012; orange dots), Stephens et al. (2017; red dots), Weidner et al. (2013a; gray dots), and Ramírez Alegría et al. (2016; blue dots), where Weidner et al. (2013a) is an inhomogeneous set of data culled from the literature for very young clusters without supernova remnants. The average $M_{\rm ecl}$ uncertainty is 0.34 dex; the average $m_{\rm str,max}$ uncertainty, 0.16 dex, is indicated by gray dots and light gray indicates data points with larger uncertainties. The thin solid line indicates the $M_{\rm ecl}$ = $m_{\rm str,max}$ limit and the horizontal thin dashed line indicates the 150 $M_\odot$ limit in our Eq. (4).

In the present paper, we focus on studying optimal sampling on the galactic scale for the first time. It is worth noting that the mathematical formulation of optimal sampling has been improved by Schulz et al. (2015, hereafter SPK). We followed the formulation of SPK in this paper even though the original formulation leads to insignificantly different results. The core idea of optimal sampling is not mathematical idealism but to develop a deterministic sampling method that can describe what a self-regulated nature would do to account for the small scatter of the observations. When choosing a sampling method for the numerical initialization of stellar systems, it is most important to consider that the sampled result is consistent with a variety of observations. We demonstrate later that this is exactly what the OSGIMF model achieves.

The paper is organized as follows: in Sect. 2, the assumptions underlying the IGIMF theory and optimal sampling are described. The python module, GalIMF, which we developed to simulate the theory, is described in Sect. 3; we make this module available for general use. The results from GalIMF are presented in Sect. 4 and are compared with observations. Sections 5 and 6 contain the discussion and conclusions, respectively.

Table 1. Notation.

Notation	Meaning
m	Integration variable for stellar mass
$m_{\rm max}$	Integration upper limit for stellar mass
$m_{\rm min}$	Integration lower limit for stellar mass
$m_{\rm str}$	Stellar mass
$m_{\rm str,max}$	Most massive stellar mass
M	Integration variable for star-cluster mass
$M_{\rm max}$	Integration upper limit for cluster mass
$M_{\rm min}$	Integration lower limit for cluster mass
$M_{\rm ecl}$	Embedded star-cluster mass
$M_{\rm ecl,max}$	Most massive embedded star-cluster mass
$M_{\rm cl}$	Mass of the pre-cluster molecular cloud

2. Model

2.1. The integrated galaxy-wide IMF

The underlying idea of the IGIMF theory is overly simple and realistic. The IMFs assembled in star-forming regions must add up to the IMF of the whole galaxy; i.e., first a series of embedded star clusters is generated from the ECMF, then a series of stars for each embedded cluster is generated from the IMF and, finally, stars from all the clusters are summed up to generate the galaxy-wide IMF.

To formulate the IGIMF theory, we assumed the following five axioms (see also Recchi & Kroupa 2015; Fontanot et al. 2017[2], for comparison) with notation clarified in Table 1. We used different symbols for integration variable and object mass. The integration variable applies to the continuous mass distribution function while the object mass applies to the discretized sampled mass.

Axiom 1:

Every star in the galaxy is generated in an embedded cluster.

This assumption is physically plausible because stars form in molecular cloud overdensities that contain much more mass than the mass of the least massive star ($\approx$0.08 $M_\odot$). This means when a gas cloud collapses to form stars it always forms more than one star, following the particular stellar IMF. Stars in small embedded clusters, for example, $M_{\rm ecl} < 50\ M_\odot$ or so, quickly dissolve into the galaxy and may be observed as a distributed young stellar component (e.g., Kroupa & Bouvier 2003). Observations indeed suggest that most and perhaps all the observed stars were formed in embedded clusters (Lada & Lada 2003; Kroupa 2005; Megeath et al. 2016). The properties of galactic-field binary stars also suggest this to be the case (Kroupa 1995a,b).

Axiom 2:

We define two functions describing (a) the mass distribution of stars that follows the stellar IMF, $\xi_\star(m) = {\rm d}N_\star/{\rm d}m$, where ${\rm d}N_\star$ is the number of stars with mass in the range m to $m + {\rm d}m$, and (b) the embedded cluster mass distribution in the galaxy that follows the ECMF, $\xi_{\rm ecl}(M) = {\rm d}N_{\rm ecl}/{\rm d}M$, where ${\rm d}N_{\rm ecl}$ is the number of embedded clusters with mass in stars in the range M to $M + {\rm d}M$. Then the stellar mass function for the whole galaxy is the sum of stars in all embedded clusters and can therefore be integrated as

$$\xi_{\rm IGIMF}(m, SFR) = \int_0^{+\infty} \xi_\star(m, M)\, \xi_{\rm ecl}(M, SFR)\, {\rm d}M, \tag{1}$$

where SFR is the star formation rate and $\xi_{\rm ecl}(M, SFR)$ is defined in Eq. (9) below.

This formalism represents a general prescription for the construction of the galaxy-wide IMF from locally valid stellar IMFs. It specifically implies that even if the IMF is universal and fixed on the star-cluster scale, the galaxy-wide IMF can vary. As an extreme example, 1000 small star clusters of 10 $M_\odot$ would have the same total mass but a different stellar population than a single 10^4 $M_\odot$ star cluster, simply because all stars more massive than 10 $M_\odot$ only exist in the latter case.

Axiom 3:

The stellar IMF, $\xi_\star(m)$, is canonical (Kroupa 2001) if the embedded cluster is forming in a gas cloud with a molecular cloud core density $\rho_{\rm cl} < 9.5 \times 10^4$ [$M_\odot\,{\rm pc}^{-3}$], where the molecular cloud core density accounts for the mass of stars and gas as defined in Eq. (6) below, following Marks et al. (2012):

$$\xi_\star(m, M) = \begin{cases} 0, & m < 0.08\ M_\odot, \\ 2k_\star m^{-1.3}, & 0.08\ M_\odot \leqslant m < 0.5\ M_\odot, \\ k_\star m^{-2.3}, & 0.5\ M_\odot \leqslant m < 1\ M_\odot, \\ k_\star m^{-\alpha_3}, & 1\ M_\odot \leqslant m < m_{\rm max}(M), \\ 0, & m_{\rm max}(M) \leqslant m, \end{cases} \tag{2}$$

where $\alpha_3 = 2.3$ is the constant Salpeter-Massey index for the invariant canonical IMF but changes for larger $\rho_{\rm cl}$ to account for IMF variation under starburst conditions (Elmegreen & Shadmehri 2003; Shadmehri 2004; Dib et al. 2007; Dabringhausen et al. 2009, 2012; Marks et al. 2012). The value 0.08 $M_\odot$ in Eq. (2) is about the lower mass limit of stars (Thies et al. 2015).

The parameters $k_\star$ and $m_{\rm max}$ in Eq. (2) are determined simultaneously by solving Eqs. (3) and (4) together, i.e., using the mass conservation of the embedded cluster

$$M_{\rm ecl} = \int_{0.08\ M_\odot}^{m_{\rm max}} m\, \xi_\star(m)\, {\rm d}m, \tag{3}$$

and the optimal sampling normalization condition, which is explained at the end of Axiom 4,

$$1 = \int_{m_{\rm max}}^{150\ M_\odot} \xi_\star(m)\, {\rm d}m, \tag{4}$$

where 150 $M_\odot$ is the adopted stellar upper mass limit (Weidner & Kroupa 2004; Figer 2005; Oey & Clarke 2005; Koen 2006; Maíz Apellániz et al. 2007). Higher mass stars are most likely to be formed through mergers (Banerjee et al. 2012a,b).

For larger $\rho_{\rm cl}$, $\xi_\star(m)$ becomes top heavy where a $\alpha_3(\rho_{\rm cl})$ relation is adopted from Marks et al. (2012),

$$\alpha_3 = \begin{cases} 2.3, & \rho_{\rm cl} < 9.5 \times 10^4, \\ 1.86 - 0.43 \log_{10}(\rho_{\rm cl}/10^6), & \rho_{\rm cl} \geq 9.5 \times 10^4. \end{cases} \tag{5}$$

Here

$$\rho_{\rm cl} = 3M_{\rm cl}/4\pi r_{\rm h}^3 \tag{6}$$

[2] We believe there are some typos in Fontanot et al. (2017). In their Eq. (5), the number –1.06 should be –0.106; in their Eq. (6), the number 2.35 should be 2.3 and 10^4 should be 10^6. Corresponding to their Eq. (7), $M_{\rm cl}$ is $M_{\rm ecl}$ in our notation.

in the unit of $[M_\odot/\mathrm{pc}^3]$ is the pre-cluster molecular cloud core density when the embedded cluster is forming, where $M_{\rm cl}$ is the original molecular cloud core mass including gas and stars and $r_{\rm h}$ is the formal half-mass radius of the embedded cluster at its theoretical birth time (see Marks & Kroupa 2012). Observed binary star distribution functions constrain the birth density of the cluster.

For a star formation efficiency of 33%, $M_{\rm cl}$ is three times the mass of the embedded cluster, $M_{\rm ecl}$. From Marks & Kroupa (2012) we adopt $\log_{10}\rho_{\rm ecl} = 0.61\log_{10}M_{\rm ecl} + 2.08$ and $r_{\rm h}/\mathrm{pc} = 0.1M_{\rm ecl}^{0.13}$, where $M_{\rm ecl}$ is in the unit of $[M_\odot]$. Together with $\rho_{\rm ecl} = 3M_{\rm ecl}/4\pi r_{\rm h}^3$ (here the subscript, ecl, is different from Eq. (6), cl.) five relations and five unknown parameters lead to

$$\log_{10}\rho_{\rm cl} = 0.61\log_{10}M_{\rm ecl} + 2.85. \tag{7}$$

The star formation efficiency of 33% is reasonable but not strict (Banerjee & Kroupa 2015; Megeath et al. 2016) and the original molecular cloud core density is not observable. In fact, here we have an empirical relation between α_3 and $M_{\rm ecl}$ (combining Eqs. (5) and (7)) that is derived from star cluster observations without a metallicity selection.

Although Eq. (5) only depends on $\rho_{\rm cl}$, it does not suggest that a fixed solar metallicity assumption is applied because there is a correlation between the metallicity and $\rho_{\rm cl}$ (Telford et al. 2016[3]). A decomposed empirical relation considering the metallicity environment specifically can also be adopted from Marks et al. (2012). We refer to this as the $\alpha_3(x)$ relation

$$\alpha_3 = \begin{cases} 2.3, & x < -0.87, \\ -0.41x + 1.94, & x > -0.87, \end{cases} \tag{8}$$

where $x = -0.14[\mathrm{Fe/H}] + 0.99\log_{10}(\rho_{\rm cl}/10^6)$. An independent observational evidence for this $\alpha_3(x)$ variation in Eq. (8) is given by a recent analysis of star clusters in M 31 (Zonoozi et al. 2016; Haghi et al. 2017).

Applying Eqs. (8) instead of (5) affects the high mass end of the IMF and the high mass end of all the following results (Figs. 3 to 6), but only slightly. Here we choose Eq. (5) as our fiducial model and Eq. (8) with fixed solar metallicity ([Fe/H] = 0) as the SolarMetal model. The SolarMetal model is only considered as a robustness check shown in our final result (Fig. 6) and Appendix B. In general, the fiducial model should be more reliable than a constant metallicity assumption although the difference is not significant for metallicities close to solar value.

With the α_3–$\rho_{\rm cl}$ relation (Eq. (5)) and the $\rho_{\rm cl}$–SFR relation that high SFR galaxies form star clusters that extend to larger masses and thus to higher cloud core densities (see Eqs. (11), (13) and (7)), it follows that the IGIMF becomes top heavy for high galaxy-wide SFRs. This is demonstrated in Fig. 3 below.

Axiom 4:

The ECMF is a single slope power law with a variable power-law index, β, that depends on the SFR of the galaxy:

$$\xi_{\rm ecl}(M, SFR) = \begin{cases} 0, & M < M_{\rm min}, \\ k_{\rm ecl}M^{-\beta(SFR)}, & M_{\rm min} \leqslant M < M_{\rm max}(SFR), \\ 0, & M_{\rm max}(SFR) \leqslant M, \end{cases} \tag{9}$$

where $M_{\rm min} = 5\ M_\odot$ is the assumed lower limit of embedded cluster masses roughly corresponding to the smallest stellar groups observed (Kirk & Myers 2012; Kroupa & Bouvier 2003), $M_{\rm max}$ is the upper integration limit in the optimal sampling method defined in SPK and $k_{\rm ecl}$ is a normalization constant. The determination of these parameters is detailed below.

Following Weidner et al. (2013b), we assumed the ECMF to be flattened (top heavy) for galaxies with a high SFR,

$$\beta = -0.106\log_{10}SFR + 2, \tag{10}$$

where SFR is in the unit of $[M_\odot/\mathrm{yr}]$.

The single slope power-law assumption (Eq. (9)) is suggested by observation (Lada & Lada 2003). The actual shape of the ECMF might be more complicated, for example, a Schechter-type form that follows the single power-law form at the low mass end but turns down rapidly at the high mass end (see Lieberz & Kroupa 2017). This kind of modification does not significantly influence the conclusions of the present paper.

The sensitive assumption here is Eq. (10), which directly links to the dependency of the IGIMF shape on the SFR (i.e., the IGIMF-shape–SFR relation in Fig. 3 below). The power-law index β was observationally found to lie between 1.5 and 2.5 (Weidner et al. 2004) which is consistent with Eq. (10) for $-5 < \log_{10}(SFR/[M_\odot/\mathrm{yr}]) < 5$. However, our assumption differs from Weidner et al. (2013b) as they only use Eq. (10) for $SFR > 1\ M_\odot\,\mathrm{yr}^{-1}$ instead of for every SFR. This is because adopting the β–SFR relation (Eq. (10)) for all SFRs naturally fits the observationally suggested $\alpha_3^{\rm gal}$–SFR relation for galaxies and our result is actually similar to Weidner et al. (2013b), which is shown later in Fig. 6. The difference in IGIMF shape between applying our β–SFR relation assumption and that of Weidner et al. (2013b) is shown in Figs. 3 and B.2, respectively.

Again, the parameters $k_{\rm ecl}$ and $M_{\rm max}$ in Eq. (9) are determined by solving Eqs. (11) and (12) together, i.e., by invoking the embedded cluster population mass conservation,

$$M_{\rm tot} = \int_{M_{\rm min}}^{M_{\rm max}} M\,\xi_{\rm ecl}(M)\,\mathrm{d}M, \tag{11}$$

where $M_{\rm tot}$ is the stellar mass formed within time δt, which is introduced in Eq. (13), and the optimal sampling normalization condition,

$$1 = \int_{M_{\rm max}}^{10^9\ M_\odot} \xi_{\rm ecl}(M)\,\mathrm{d}M, \tag{12}$$

where the upper integration limit of $10^9\ M_\odot$ is the hypothetical physical upper bound of embedded cluster mass roughly corresponding to the limit at which stellar-dynamical systems of star-cluster type (ultracompact dwarf galaxies) appear to end (e.g., Dabringhausen et al. 2008).

Originally, the normalization form of Eq. (12) comes from the notion that there is exactly one object in the mass range from $M_{\rm max}$ to $10^9\ M_\odot$. But according to the method of SPK, an embedded cluster is not actually generated in this mass range. So this normalization method is only justified by its ability to describe observations. It can be seen in Figs. 1 and 2 below, respectively, that the generated maximum stellar and embedded cluster mass, $m_{\rm str,max}$ and $M_{\rm ecl,max}$[4], fit well with the observational constraints. It is possible to modify the hypothetical upper mass limit or the value on the left-hand side of Eq. (12) to change the resulting $M_{\rm ecl,max}$–SFR relation and fit the data but this is not a concern of the present paper.

[3] Telford et al. (2016) conclude a metallicity–SFR relation of galaxies, while SFR correlates with $\rho_{\rm cl}$ according to our Axiom 4 and Axiom 5 below.

[4] The meaning of the symbols and notation is listed in Table 1.

Axiom 5:

An ensemble of embedded clusters that optimally populate the ECMF is formed in a $\delta t = 10$ Myr period with a constant SFR. This is reasonable because, although the short-term fluctuation of the local (<few pc scale) SFR can happen on a dynamical timescale of less than one to a few Myr, a stable long-term galaxy-wide variation typically happens on a timescale of a few hundred Myr (see Renaud et al. 2016, for interacting galaxies). The period δt is called a star formation epoch and we have the following relation:

$$M_{\rm tot} = SFR \cdot \delta t, \tag{13}$$

where $M_{\rm tot}$ is the total stellar mass of embedded clusters formed in δt throughout the galaxy.

The value $\delta t \approx 10$ Myr accounts for the typical observationally deduced galaxy-wide interstellar medium (ISM) timescale of transforming the ISM via molecular clouds into a new stellar population (Egusa et al. 2004, 2009; review: Fukui & Kawamura 2010; Meidt et al. 2015). The disappearance of large molecular clouds around young star clusters also takes about 10 Myr (Leisawitz 1989). In our model, δt was actually determined by the empirical $M_{\rm ecl,max}$–SFR relation as a larger δt results in a larger $M_{\rm ecl,max}$, which can violate the $M_{\rm ecl,max}$–SFR relation. This work and previous work (Weidner et al. 2004; SPK) have tested that the 10 Myr epoch assumption reproduces the observed $M_{\rm ecl,max}$–SFR relation. This consistency between the observationally estimated ISM timescale and the δt needed to fit the observational $M_{\rm ecl,max}$–SFR data is noteworthy and encouraging.

2.2. The optimally sampled galaxy-wide IMF

As opposed to making an integration and resulting in a smooth function with our Axiom 2, a sampling procedure gives a discrete list of stellar masses. We used the optimal sampling method from SPK, their Eqs. (1) to (7) and (9), where their symbol $M_{\rm max}$ is $M_{\rm max}$ or $m_{\rm max}$ here, and $M_{\rm trunc}$ in their paper is set to be $10^9\ M_\odot$ and 150 $M_\odot$ in our Eqs. (12) and (4), respectively. More details about the sampling method are provided in SPK. Here we only highlight some important points as SPK made some improvements on the optimal sampling formalism.

In the SPK method, the mass upper integration limit is not the most massive object mass itself but the upper integration limit of the most massive object. This means the mass of the most massive embedded cluster, $M_{\rm ecl,max}$[5], in the empirical $M_{\rm ecl,max}$–SFR relation is not the upper mass limit $M_{\rm max}$ in Eq. (11). Rather, $M_{\rm max}$ is calculated by Eq. (9) in SPK. The empirical $M_{\rm ecl,max}$–SFR relation is automatically fulfilled if $\delta t = 10$ Myr as stated in Axiom 3. This is shown in Fig. 2 below.

The case of sampling stars within an embedded cluster is similar. The mass of the most massive star in an embedded cluster, $m_{\rm str,max}$[6], in the empirical $m_{\rm str,max}$–$M_{\rm ecl}$ relation is not used as the upper integration limit, $m_{\rm max}$, in Eq. (3). The SPK optimal sampling formalism with a stellar truncation mass of 150 $M_\odot$ automatically fulfills the $m_{\rm str,max}$–$M_{\rm ecl}$ relation as is shown in Fig. 1 below.

The new SPK sampling formalism is more reasonable in the sense that physical mass is only the integration result rather than being the integration upper limit. In addition, the SPK formalism reduces the number of assumptions for the model. The $M_{\rm ecl,max}$–SFR relation becomes a natural result of optimal sampling instead of an assumption; see, for example, Weidner et al. (2013b, their axiom (5)).

[5] $M_{\rm ecl}$ stands for the actual embedded cluster mass in stars obtained from observation or sampled by our code. The value $M_{\rm ecl,max}$ explicitly indicates the most massive cluster mass instead of an upper integration limit such as $M_{\rm max}$. See Table 1.

[6] The value $m_{\rm str}$ stands for the actual stellar mass similar to $M_{\rm ecl}$.

3. The publicly available module: GalIMF

A freely available Python code, GalIMF, was developed to compute the IGIMF and the OSGIMF for a given galaxy-wide SFR and metallicity.

The current version, GalIMF version 1.0.0, incorporates the axioms as detailed in Sect. 2. Modifications, for example, allowing the stellar IMF to vary with metallicity below 1 $M_\odot$ as described in Marks et al. (2012), are easy to implement by changing the model number flags.

GalIMF version 1.0.0 developed for the current paper is available at CDS or at GitHub[7]. Code usage example, gallery, and future version of GalIMF are available at GalIMF homepage[8].

4. Results

With GalIMF, we confirm the previous studies that the IGIMF theory, with and without a discretization by sampling procedure, is consistent with the observed $m_{\rm str,max}$–$M_{\rm ecl}$, $M_{\rm ecl}$–SFR and $\alpha_3^{\rm gal}$–SFR relations, where $\alpha_3^{\rm gal}$ is the effective power-law index of the galaxy-wide IMF for stars above 1 $M_\odot$ and SFR is the galaxy-wide SFR. An inference relation between the galaxy-wide SFR and Type II supernova (SNII) occurrence is given as a test of the OSGIMF theory.

The OSGIMF, which is the discretized version of the IGIMF, shows additional serrated features that only appear when the deterministic sampling, for example, optimal sampling[9] with a large ECMF slope of $\beta > 2.1$ is applied.

4.1. $m_{\rm str,max}$–$M_{\rm ecl}$

The $m_{\rm str,max}$–$M_{\rm ecl}$ relation for the optimally sampled result is shown in Fig. 1 for comparison with the observations. We plot not only the most massive but also the second and third massive sampled stellar mass. Stellar ejections and mergers (Oh & Kroupa 2012, and in prep.) may alter the relation calculated from optimal sampling.

A steepening feature appears in the $m_{\rm max}$–$M_{\rm ecl}$ relation at $M_{\rm ecl} > 10^{3.49}\ M_\odot$ if the $\alpha_3(\rho_{\rm cl})$ relation (Eq. (5)) is used (also shown as thin lines in Fig. C.1) when compared to the flatter $m_{\rm str,max}$–$M_{\rm ecl}$ relation at $M_{\rm ecl} > 10^{3.49}\ M_\odot$ if $\alpha_3 = $ const. (thick lines in Fig. C.1). This steepening, although not so pronounced, is critical to understand a spoon feature in Fig. 4 that is discussed in Sect. 4.4 and Appendix C.

The data points come from different papers. Clusters in Stephens et al. (2017) have been estimated to have an age younger than 5 Myr. We used the average values of "1 Myr estimated" and "2.5 Myr estimated" $M_{\rm ecl}$ found in Table 6 in Stephens et al. (2017). The uncertainty of $M_{\rm ecl}$ comes from the

[7] https://github.com/Azeret/galIMF

[8] https://sites.google.com/view/galimf/home

[9] Optimal sampling as introduced in Kroupa et al. (2013) and improved by Schulz et al. (2015) is not the only possible formalism for a deterministic sampling. There are other deterministic ways to sample a distribution and yield different results; for example, one could modify the current optimal sampling normalization condition.

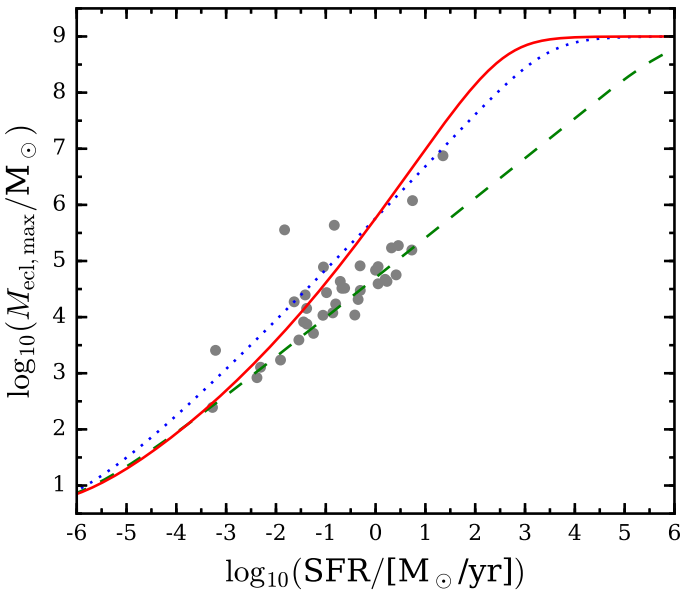

Fig. 2. Most massive young cluster mass to galaxy-wide SFR ($M_{\rm ecl,max}$–SFR) relation. The optimally sampled results for different β are shown as a red solid curve for β following Eq. (10), blue dotted curve for $\beta = 2$, and green dashed curve for $\beta = 2.4$. Observational data (gray dots) adopted from Weidner et al. (2004) have a typical uncertainty of 0.3 dex. The $\beta = 2$ and 2.4 curves are almost identical with Fig. 6 in Weidner et al. (2004; middle dotted and middle dashed curves, respectively), in which the $\delta t = 10$ Myr assumption is also adopted. See also Randriamanakoto et al. (2013).

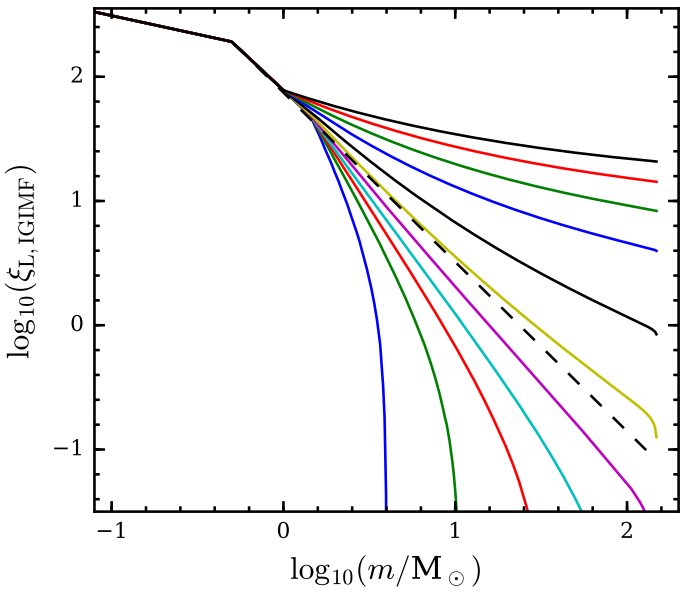

Fig. 3. Logarithmic integrated galaxy-wide IMFs, $\xi_{\rm L,IGIMF}$ (Eq. (14)), for different SFRs and formed over a 10 Myr epoch. The unit of $\xi_{\rm L,IGIMF}$ is the number of stars per log-mass interval. Each line is normalized to the same values at $m < 1\ M_\odot$. Solid curves are IGIMFs for galactic $SFR = 10^{-5}, 10^{-4} \ldots 10^{5}\ M_\odot$/yr from bottom left to top right. The dashed line is the canonical IMF (Eq. (2)) with $\alpha_3 = 2.3$. The lines lower than the dashed line deviate from the canonical IMF above 1.1 $M_\odot$ which is the most massive stellar mass in the least massive embedded clusters $M \approx M_{\rm min} = 5\ M_\odot$. The lines on top of the dashed line deviate from the canonical IMF above 1 $M_\odot$, which is the lower mass limit for applying α_3 as defined in Eqs. (2) and (5). This plot is comparable with earlier IGIMF works from Weidner et al. (2013b) and Fontanot et al. (2017).

estimation of the cluster ages and the resulting $M_{\rm ecl}$ error is approximately from a normal distribution with a 2σ certainty range of about ±44%, or $+0.158/-0.252$ dex according to the description in their Sect. 5.3. But their $M_{\rm ecl}$ is likely to be underestimated because of extinction and the effect is unclear. Thus we assumed an overall error according to a normal distribution in the logarithmic scale with standard deviation $\sigma = 0.126$ dex. In Stephens et al. (2017), the $m_{\rm max}$ values can be overestimated because of the multiplicity of the stars and underestimated due to extinction and the fact that the stars may still be accreting. In addition, the $m_{\rm max}$ estimation in Stephens et al. (2017) has several other ambiguous processes and these authors did not provide an error (see their Sect. 4.3). Thus we assumed an overall error according to a normal distribution in the logarithmic scale with standard deviation $\sigma = 0.13$ dex. We adopt the top panel of Fig. 13 in Kirk & Myers (2012). The mass estimations have an uncertainty of order 50% as stated in Kirk & Myers (2011, their Sect. 2.1), which is $+0.176/-0.301$ dex. Weidner et al. (2013a) have collated an inhomogeneous set of data culled from the literature for very young clusters without supernova remnants. The catalog contains only clusters with age below 5 Myr to exclude the possibility that the most massive star has already exploded as a supernova and no other selection criterion was applied. The average $M_{\rm ecl}$ uncertainty is ±0.34 dex and the average $m_{\rm str,max}$ uncertainty is ±0.16 dex for the data from Weidner et al. (2013a). The uncertainties of the $M_{\rm ecl}$ and $m_{\rm str,max}$ data points are calculated and the data points are plotted in Fig. 1 with a different shade of gray, where lighter indicates larger uncertainties[10]. The blue data points from Ramírez Alegría et al. (2016, their Fig. 11) are five young clusters that have ages older than the other data presented here. Their ages are roughly up to 10, 7.5, 9, 20, and 7 Myr for data points from left to right. The largest discrepancy for this sample from our model is also the oldest cluster (i.e., 20 Myr), which may already have lost its most massive star though stellar evolution or dynamical ejection. A stellar mass estimation error is not provided by Ramírez Alegría et al. (2016). These data follow the dotted line, as expected for such older clusters.

The observational data points in Fig. 1 show no evidence for an intrinsic scatter and support the optimal sampling scenario. This statement is well established in Weidner et al. (2013a, their Fig. 1) by showing most of the observational data lie within the region where only 66% of them should lie if stars were randomly sampled from the IMF. A further quantitative discussion disfavoring the random sampling scenario has been performed in Yan et al. (in prep.) with randomly sampled $m_{\rm str,max}$–$M_{\rm ecl}$ relations directly compared with the observations. The scatter of the data points is shown to be significantly smaller than random sampling from the IMF and is consistent with no intrinsic scatter given the observational uncertainties.

4.2. $M_{\rm ecl}$–SFR

The $M_{\rm ecl}$–SFR relation for our sampled result is shown in Fig. 2. The data points provided by Weidner et al. (2004) comprise a homogeneous data set of galaxies with young star clusters. The uncertainties of these data points are about 0.5 dex and 0.2 dex for cluster mass and SFR, respectively. The cluster masses in this data set are calculated from a magnitude-mass relation assuming the fixed canonical IMF. Hence, this data is consistent with the present analysis when $SFR < 0.1\ M_\odot$/yr. For higher SFRs, our $|\alpha_3|$ becomes smaller according to Eq. (5); this can be seen

[10] The light gray data points are slightly larger for better visibility.

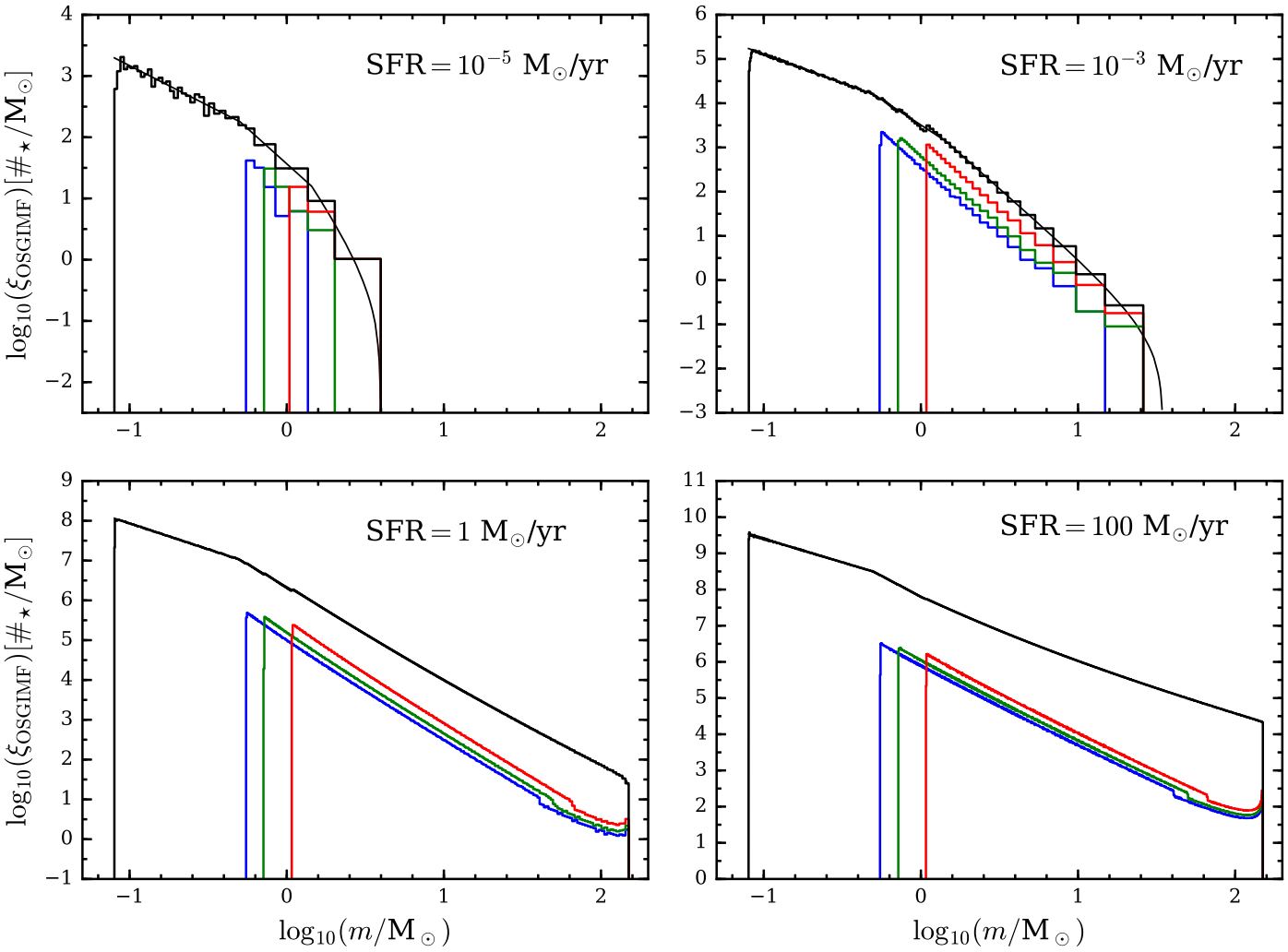

Fig. 4. Optimally sampled galaxy-wide IMFs for different SFRs. The unit of $\xi_{\rm OSGIMF}$ is the number of stars per linear mass interval. The black histogram is the entire stellar sample in the galaxy formed in a 10 Myr epoch. The large scatter in the *upper left panel* and the serrated feature around $\log_{10}(m/M_\odot) = 0$ for every panel is explained in the text. The red, green, and blue histograms, comprising our decomposition plot, are the OSGIMFs counting only the first, second, and third most massive stars of embedded clusters. A spoon feature appears at the high mass end of the red, green, and blue curves. The stellar mass distribution is saturated at the high mass end because of the 150 $M_\odot$ limit. The thin smooth curves are the IGIMFs as in Fig. 3, calculated by Eq. (1) and normalized to give the mass in stars when integrated over the relevant stellar mass ranges.

explicitly from our Fig. 5 where the lines for $SFR > 10^{-1}$ $M_\odot$/yr drop down at $\log_{10} m/M_\odot = 0$. The $M_{\rm ecl}$ values derived with our α_3 assumption would be smaller than the data adopted from Weidner et al. (2004) with their canonical α_3 assumption. It is possible that the additive constant "2" in Eq. (10) is larger; this would fit the data points better, i.e., closer to the green dashed line rather than the blue dotted line and this also makes the fiducial model higher in Fig. 6 below. Randriamanakoto et al. (2013) extend the observation of the empirical relation between the brightest cluster magnitude in a galaxy and the host SFR to higher SFRs. As the α_3–SFR dependence makes the $M_{\rm ecl}$ determination from magnitude very complicated, we do not add this data set to our plot. But Randriamanakoto et al. (2013) explicitly note that the small scatter of their data is inconsistent with random sampling from the ECMF, corroborating on the conclusion reached using different data by Pflamm-Altenburg et al. (2013).

The data points in Fig. 2 again display a small scatter that is consistent with the scenario of a highly self-regulated behavior on galaxy scales (see Disney et al. 2008; and Kroupa 2015, for a relevant discussion). In addition, our result suggests that a variable β assumption (Eq. (10)), shown by the red solid curve, fits better with the observations and may be superior to a constant β assumption, as indicated by the green dashed curve and blue dotted curve. This result supports our assumed β–SFR relation in Eq. (10), which applies to all SFRs.

4.3. Integrated galaxy-wide IMFs

The calculated IGIMFs for different SFRs are shown in Fig. 3 and can be compared with previous IGIMF works from Weidner et al. (2013b) and Fontanot et al. (2017). Here we define the logarithmic IMF,

$$\xi_{\rm L,IGIMF}(m) = \frac{{\rm d}N}{{\rm dlog}_{10}\, m} = m\ \ln(10)\ \xi_{\rm IGIMF}(m), \qquad (14)$$

where dN is the number of stars in the logarithm mass interval $\log_{10} m$ to $\log_{10} m + {\rm d}\log_{10} m$ and $\xi_{\rm IGIMF}$ is defined in Eq. (1). Our result differs slightly from the previous papers because of our newly applied improved optimal sampling formalism following SPK, as explained in Sects. 2.2 and 5.

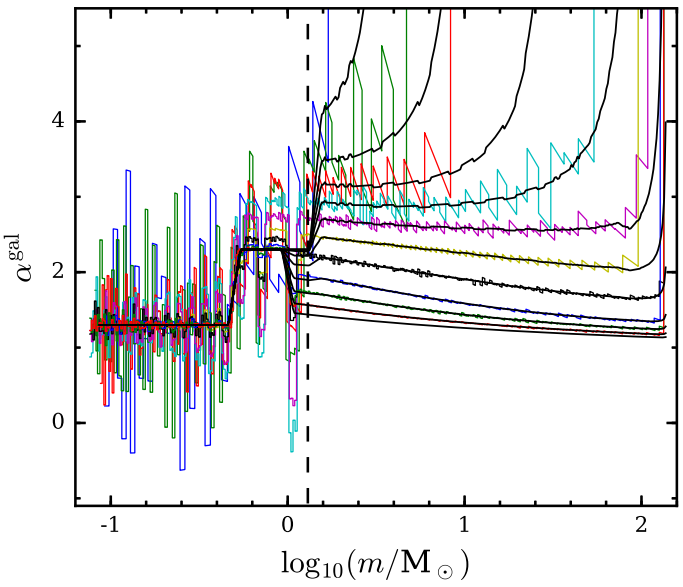

Fig. 5. Galaxy-wide IMF power-law index, $\alpha^{\rm gal}$ (Eq. (15)), for OSGIMF (colored thin lines) and IGIMF (black lines) for $SFR = 10^{-5}$, 10^{-4} ... 10^{5} $M_\odot$/yr from upper to lower lines. For the $SFR = 10^{5}$ $M_\odot$/yr case, only the IGIMF index is plotted because a star-by-star sampling costs too much computational time. Below 1 $M_\odot$, the plot reproduces the canonical IMF indexes of 1.3 and 2.3 as defined in Eq. (2). Between 1 and 1.1 $M_\odot$, $\alpha^{\rm gal}$ follows the variable α_3 defined in Eq. (5). At higher masses, $\alpha^{\rm gal}$ varies with SFR. The OSGIMF index deviates from the IGIMF index at roughly 1 $M_\odot$. This result may lead to a large observational scatter at intermediate and high mass ranges. The large $\alpha^{\rm gal}$ scatter for the OSGIMF at the low mass end and low SFR has been explained in the text for Fig. 4. The vertical dashed line at $m = 1.3$ $M_\odot$ divides the IGIMF into two parts as mentioned in Sect. 5.1.

The result shows top-heavy IMFs for high SFR galaxies and bottom-heavy IMFs for low SFR galaxies. This behavior is consistent with recent observational constraints from low mass X-ray binaries (Peacock et al. 2017).

Figure 3 also implies that galaxies with a small SFR do not form massive stars. For instance, a galaxy with a $SFR = 10^{-4}$ $M_\odot$/yr forms no stars more massive than 10 $M_\odot$ as we discuss in Sect. 4.7.

4.4. Optimally sampled galaxy-wide IMFs

The OSGIMF provides the specific masses for all the individual stars in a simulated stellar system and tightly follows the IGIMF. The OSGIMF for different SFRs are shown in Fig. 4 with the IGIMF overlaid, where the IGIMFs are the same as in Fig. 3 but here normalized to $M_{\rm tot}$ by Eqs. (11) and (13).

The difference between the IGIMF and the OSGIMF is an additional serrated feature in the latter, arising from optimal sampling on the assumed ECMF with a sharp minimum edge at $M_{\rm min} = 5$ $M_\odot$. With optimal sampling, the large number of minimum mass embedded clusters have a similar most massive star mass. This is demonstrated by the decomposition plots of the OSGIMF in red, green, and blue, counting only the first, second, and third massive stars of the embedded clusters, respectively; i.e., the left edge of the red histograms in Fig. 4 is formed by the most massive stars in all the embedded clusters that have masses close to $M_{\rm ecl,min}$. According to optimal sampling, those stars must have the same mass, leading to a sharp peak and the serrated feature around 1 $M_\odot$ that is best visible in the upper right panel and demonstrated as a derivative in Fig. 5 below (see caption of Fig. 4 and further discussions in Sect. 5.2). If a smooth changing for the ECMF lower mass limit is assumed rather than an abrupt cutoff, then the serrated feature is reduced.

The small drop down glitch, which makes the spoon feature that we mentioned above, around $\log_{10}(m/M_\odot) = 1.7$ in the decomposition plots is caused by the steepening feature of the $m_{\rm str,max}$–$M_{\rm ecl}$ relation in Fig. 1. The steepening in Fig. 1 and the spoon feature in Fig. 4 disappears if a fixed α_3 is applied, as shown in Appendix C.

The number of sampled stars shows a dispersion at the low mass end in the $SFR = 10^{-5}$ $M_\odot$/yr panel, which originates from optimal sampling. Remember, we first discretely sampled clusters, then we discretely sampled stars for each cluster. Therefore, there are stars with very similar stellar masses from clusters with different masses. The scatter is not Poissonian and is prominent at the low mass end of the stellar mass function only because the bin size is sufficiently small.

4.5. α plot

We define the incident galaxy-wide IMF power-law index or slope as:

$$\alpha^{\rm gal}(m) = -\frac{\mathrm{d}(\log_{10}\xi_{\rm GIMF})}{\mathrm{d}(\log_{10} m/M_\odot)}, \tag{15}$$

where $\xi_{\rm GIMF}$ can be the integrated galaxy-wide IMF, $\xi_{\rm IGIMF}$, or the optimally sampled galaxy-wide IMF, $\xi_{\rm OSGIMF}$. The alpha-plot (Kroupa 2001) for the OGIMF and the IGIMF for different SFRs is shown in Fig. 5 as colored lines and black lines, respectively. The figure shows a diversion at the high mass end for different SFRs and a systematic fluctuation around 1 $M_\odot$, which is caused by the serrated feature mentioned above.

4.6. $\alpha_3^{\rm gal}$–SFR

Figure 6 is the extracted $\alpha_3^{\rm gal}$–SFR relation ($\alpha_3^{\rm gal}$ is $\alpha^{\rm gal}$ in Eq. (15) for $m > 1$ $M_\odot$) from the alpha-plot (Fig. 5) at different stellar masses, m, where the IGIMF is curved and cannot be described by a single power law. As each m value gives a different $\alpha_3^{\rm gal}$–SFR relation, we plot a few lines from black to gray for stellar masses from 1.58 to 100 $M_\odot$. Generally, we have a top-heavy IMF for high-SFR galaxies and bottom-heavy IMF for low-SFR galaxies.

Unlike the model result, the data points obtained by the respective observational studies assume a single power-law IMF model[11]. The data points should therefore not be considered as IMF power-law indices probed for a specific stellar mass range and are not directly comparable with our model. For the plotted data and our model to be directly comparable, one still needs to 1) use the current model to simulate the initial stellar population for an entire star formation history of the galaxy instead of only a star formation epoch as performed here; 2) simulate the current stellar population and galaxy spectrum with star evolution models considering the age of each star; 3) simulate the observed spectrum considering extinction and a telescope model.

[11] The models have a single power index either for the entire IMF or at the high stellar mass end.

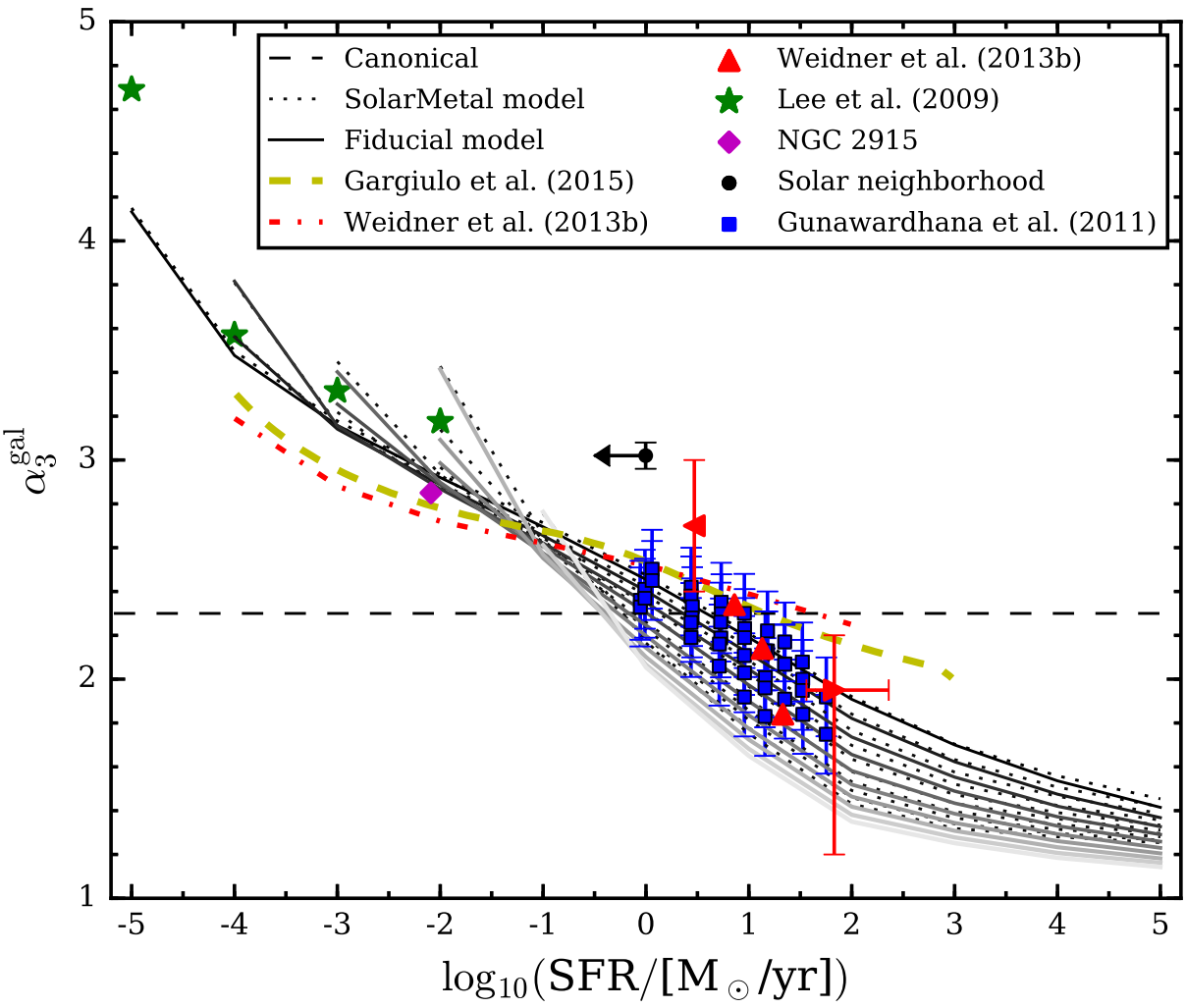

Fig. 6. Observed high mass end power-law index of the galaxy-wide IMF resulting from the calculated IGIMF, $\alpha_3^{\rm gal}$ (i.e., $\alpha^{\rm gal}$ in Eq. (15) for $m > 1\ M_\odot$), for a constant SFR over $\delta t = 10$ Myr in dependence of the galaxy-wide SFR. In Fig. 5, $\alpha_3^{\rm gal}$ values diverge for different SFRs and also vary for different m at the high mass end. As at each m value there exists a different $\alpha_3^{\rm gal}$–SFR relation, we plot solid lines for $\log_{10}(m/M_\odot) = 0.2$, 0.4, ..., 2, i.e., 1.58, 2.51, ..., 100 $M_\odot$ from black to gray (*top to bottom*) for the fiducial model and dotted lines for the corresponding SolarMetal model defined in Sect. 2.1. The blue squares are data from the GAMA galaxy survey (Gunawardhana et al. 2011). The red triangles and red dash-dotted line are data from Weidner et al. (2013b); the left triangle is for the MW field, the middle three triangles are galaxy studies, the right triangle is for the bulges of the MW and M 31, and the dash-dotted line is their IGIMF model assuming $\beta = 2$. A recent study has suggested that the 2 $M_\odot$/yr SFR for MW is overestimated (Chomiuk & Povich 2011), but we leave this data point the same as in Weidner et al. (2013b). Gargiulo et al. (2015) report consistency between their IGIMF model assuming $\beta = 2$ (thick yellow dashed line) and the [α/Fe] abundance ratios of elliptical galaxies. The purple diamond is an individual analysis for the dwarf galaxy NGC 2915 (Bruzzese et al. 2015). Green stars are based on the Lee et al. (2009) 11HUGS observations of dwarf galaxies. The black circle is an observation for the solar neighborhood from Rybizki & Just (2015) with adopted MW SFR from Robitaille & Whitney (2010) as an upper limit of the solar neighborhood SFR because the Sun is located in an inter-arm region where the relevant SFR is significantly smaller (toward the direction indicated by the arrow; see Sect. 4.6 for further details). The thin horizontal dashed line represents the canonical IMF index $\alpha_2 = \alpha_3 = 2.3$.

and 4) use the same single power-law IMF model and all other assumptions to fit the simulated observed spectrum exactly as the observational studies did. As these procedures require much more investment and may only provide similar results, we use the data points in Fig. 6 as an indicator only to show that the general trend of our model is consistent with the observational research results.

The data points of Gunawardhana et al. (2011) were extracted from the panel (a) in their Fig. 13. The data points of Lee et al. (2009) were extracted from the IGIMF model by Pflamm-Altenburg et al. (2007, their Fig. 4)[12]. Lee et al. (2009) examined 11HUGS data of far ultraviolet non-ionizing continuum and Hα nebular emission for a volume limited sample of about 300 nearby star-forming dwarf galaxies, finding a systematic change of the Hα over UV flux and concluded that the IGIMF is consistent with these 11HUGS observations, which indicate a systematic deficit of ionizing massive star in galaxies with low SFRs. The observational constraints from Lee et al. (2009) indicate an upward turn in the $\alpha_3^{\rm gal}$ curves toward very

[12] For simplicity, the α_3 value extracted here for Fig. 6 is only a characteristic value for the Pflamm-Altenburg et al. (2007) curved IGIMF shape. In principle, it should also be shown as a few lines in Fig. 6 as for our own calculation. Also, the $SFR > 2\ M_\odot$/yr part of the Pflamm-Altenburg et al. (2007) result is not adopted because their stellar IMF is fixed without the α_3 dependence assumed here in Eq. (5), which changes the IMF shape at higher SFRs.

small SFRs. This is, remarkably, a natural outcome of the IGMF theory, which was predicted by Pflamm-Altenburg et al. (2007, 2009). The data from Weidner et al. (2013b) is extracted from their Fig. 1 where they assume $\beta = 2$ and $\alpha_3(x)$ (our Eq. (8)). Gargiulo et al. (2015) checked the consistency between the IGIMF theory and [α/Fe] abundance ratios of elliptical galaxies. They use a constant-β and a preliminary version of the α_3–$M_{\rm ecl}$ relation. The middle line in their Fig. 1 (for "$\beta = 2$, $M_{\rm ecl}^{\rm min} = 5\,M_\odot$") is shown in our Fig. 6 as the yellow dashed line.

In regards to the solar neighborhood data evident in Fig. 6 that do not appear to fit the IGIMF theory, these data points are plotted using the MW $SFR \approx 1\,M_\odot$/yr estimated by Robitaille & Whitney (2010). But this Galactic estimation can be higher than the local SFR in the solar neighborhood as we are in an inter-arm region that has a relatively lower SFR than the average Galactic value as suggested by extragalactic studies (e.g., Seigar & James 2002). In addition, the local field α_3 value can also be different from $\alpha_3^{\rm gal}$. Several past studies (Kennicutt 1983; Kennicutt et al. 1994; Baldry & Glazebrook 2003) indeed reported a discrepancy between the IMF of the solar neighborhood (Scalo IMF; Scalo 1986) and other late-type galaxies similar to the MW (Salpeter IMF; Salpeter 1955). Variations of the local field IMF as a result of the changing local SFR are discussed by Elmegreen & Scalo (2006). Thus, the local field study can only be taken as a reference for the galaxy-wide SFR–$\alpha_3^{\rm gal}$ relation of the MW.

The data points shown in Fig. 6 are not direct measurements but interpretations from flux measurements, e.g., Hα/UV ratios. A variable IMF is not necessarily the only way to explain such observations. Differences in the treatments of processes or a special star formation history (SFH) may lead to similar results. However, the attempt of changing the SFH to account for the observations requires that all the observed galaxies are in-phase in their SFH (see "coordinated bursts" in Hoversten & Glazebrook 2008). As the cited studies used a large number of galaxies, this scenario becomes highly unlikely. In addition, the magnitude of SFR variation required in this special SFH scenario is unrealistic as stated by Lee et al. (2009, their Sect. 4.5). A comprehensive discussion can also be found at Gunawardhana et al. (2011, their Sect. 6).

In addition, a recent study of the Sagittarius dwarf galaxy (Hasselquist et al. 2017) performed an analysis on elemental abundances for 16 different elements on 158 red giant stars suggesting that this low SFR dwarf galaxy needed a top-light IMF.

Nevertheless, here the argument is not that the observationally suggested $\alpha_3^{\rm gal}$–SFR relation must be true, but that the apparent agreement between this suggested relation and our derived relation from the locally valid observations and our theory is remarkable. The general shape of the prediction of the IGIMF model (gray lines in Fig. 6) follows the empirical extragalactic constraints well and the results calculated here are comparable to previous work (Weidner et al. 2013b; Gargiulo et al. 2015[13]). Although the comparison with the IGIMF slopes is illustrative rather than quantitative as the observational constraints are obtained by assuming the galaxy-wide IMF to be a single power-law function, this is still particularly encouraging. We emphasize that this is a remarkable outcome because the prediction of the IGIMF model as shown in Fig. 6 is sensitive to Eqs. (5) and (10), i.e., the α_3–$\rho_{\rm cl}$ and β–SFR relations, which are independently determined by different empirical data[14]. The good agreement between the modeled $\alpha_3^{\rm gal}$–SFR relation and the observations is a natural result of the IGIMF theory.

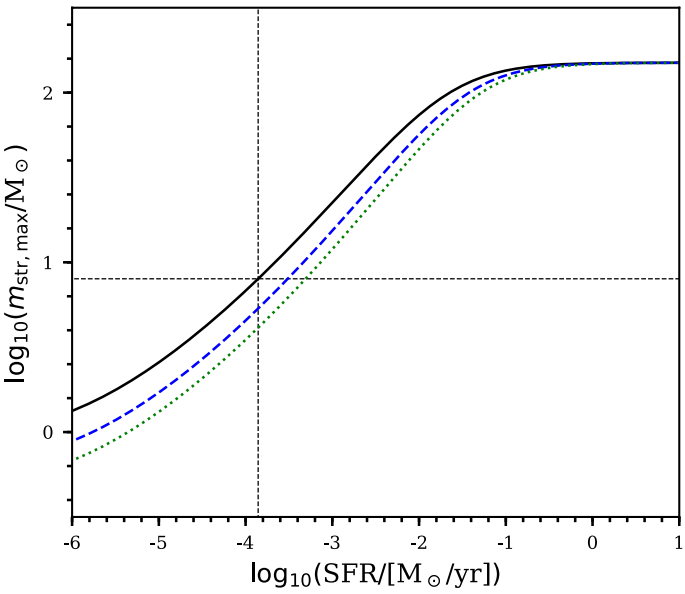

Fig. 7. Optimally sampled most-, second-, and third-massive star to be found in a galaxy as a function of the galaxy-wide SFR. These stars are shown as a solid curve, blue dashed curve, and green dotted curve, respectively, resulting from a combination of Figs. 1 and 2. The thin horizontal dashed line indicates the mass limit below which SNII explosions are not likely ($8\,M_\odot$), and the vertical thin dashed line shows the SFR below which galaxies are not expected to host SNII events, subject to the axioms adopted in the present study. See Sect. 4.7 for more details.

4.7. $m_{\rm str,max}$–SFR

Figure 7 shows the most-, second- and third-most massive star in a galaxy as a function of the SFR of the galaxy. It results from a combination of Figs. 1 and 2.

For the axioms we adopt here, Fig. 7 implies that if there were no binaries a galaxy with a $SFR < 10^{-4}\,M_\odot$/yr would have no SNII or any other core collapse supernova events, allowing a potential observational test of the IGIMF theory as axiomatized here. However, since most stars are formed as binaries some of these may merge to form a massive star despite the low galaxy-wide SFR. This can result in delayed SNII events (see Zapartas et al. 2017). Another issue that remains uncertain is that stars in some mass and metallicity ranges may implode rather than explode, faking this IGIMF-induced SNII deficit. Also, the ECMF may change its character in dwarf galaxies in that massive embedded clusters may form preferentially in disks with low-shear motions (Weidner et al. 2010), perhaps implying that below a SFR threshold the ECMF may become bimodal by containing low-mass embedded clusters and a massive one as well. In such a case the IGIMF theory remains valid since the galaxy-wide IMF remains the sum over all embedded clusters each of these contributing their own stellar IMF to the galaxy; but the predictions change with the form of the ECMF.

Nevertheless, observations of a putative deficit of SNII events in a particular complete volume of galaxies are important to test the axioms underlying the IGIMF theory. This is why

[13] They both use the assumption $\beta = 2$ while our β is 2 only when $\log_{10}(SFR) = 0$ and varies from 1.5 to 2.5. This difference makes our result steeper as shown in Fig. 6.

[14] We do simplify the empirical format of Eq. (10) in comparison with Weidner et al. (2013b) but follow the same parameters.

Fig. 7 is an important quantification for the particular set of axioms made in this study.

The occurrence of supernova within the IGIMF theory (but without the variation of α_3 as implemented by Eqs. (5) and (8) here) has been investigated in more detail by Weidner & Kroupa (2005). This is qualitatively interesting because Tsujimoto (2011) noted in his chemical modeling of the Formax dSph satellite galaxy the need for a lack of stars more massive than 25 $M_\odot$.

In summary, the OSGIMF fulfills the currently available observational requirements of the $m_{\rm str,max}$–$M_{\rm ecl}$, $M_{\rm ecl,max}$–SFR, and $\alpha_3^{\rm gal}$–SFR relations and can be applied to galaxy evolution studies. A deficit of SNII events in galaxies with low SFRs is expected.

5. Discussion

5.1. Integrated galaxy-wide IMF shape

The IGIMF shape in Fig. 3 shows a moderate difference from previous works (Weidner et al. 2013b; Fontanot et al. 2017) because our assumptions about $\alpha_3(\rho_{\rm cl})$ and β(SFR) are different and because we use an integration upper limit rather than a maximum object mass in our Eqs. (11) and (3) following SPK. For example, Eqs. (3) and (4) of Fontanot et al. (2017), their "$M_{\rm cl}^{\rm max}$" and "$m_\star^{\rm max}$" were specifically defined and used as the integration upper limit in their Eq. (8). In the present paper, these values need to be calculated by solving our equation set (11) and (12) and equation set (3) and (4). Different assumptions on $\alpha_3(\rho_{\rm cl})$ and β(SFR) result in different IGIMF shapes. We list examples in Appendix B.

The IGIMF shape can be divided into three parts as is shown in Figs. 3 and 5 as follows:

(1) Below 1.3 $M_\odot$ and given our axioms, the IGIMF shape is identical to the stellar IMF, where it has three different slopes i.e., 1.3, 2.3, and α_3. The least massive embedded clusters, $M_{\rm ecl} \approx M_{\rm min} = 5\ M_\odot$, have an optimally sampled most massive star of $\approx$1.1 $M_\odot$, and therefore every embedded cluster can populate the mass function from 0.08 $M_\odot$ to a mass that is a little larger than 1.1 $M_\odot$. Thus the lower mass end of the IGIMF is not influenced by cluster mass assignment. This changed if the IMF below 1 $M_\odot$ varies with metallicity (Eq. (3) in Kroupa 2002; Eq. (12) in Marks et al. 2012).

(2) For $m > 1.1\ M_\odot$ to part three below, $\alpha^{\rm gal}$ in Eq. (15), i.e., $\alpha_3^{\rm gal}$, does not change much as shown in Figs. 5 and 6 especially for the high SFR cases.
When $SFR < 1\ M_\odot$/yr (or equivalently $\beta > 2$ from Eq. (10)), there is a deficit of massive clusters that are able to generate massive stars. Thus the slope of the IGIMF at the high mass end, $\alpha_3^{\rm gal}$, is largely influenced by the number of massive embedded clusters, i.e., it depends on β.
When $SFR > 1\ M_\odot$/yr ($\beta < 2$), there are enough massive embedded clusters to populate the IMF fully. So a larger SFR resulting in more massive clusters would not change the shape of the galaxy-wide IMF anymore. Under this condition, $\alpha_3^{\rm gal}$ is only influenced by Eqs. (2) and (5), where the IMF index α_3 changes according to the physical condition of the molecular cloud that forms the star cluster.

(3) After the second part of the IGIMF with a relatively constant slope, the IGIMF bends down rapidly and behaves like a Schechter-type function for $SFR < 10^{-3}\ M_\odot$/yr at the high mass end.

5.2. Optimally sampled galaxy-wide IMF shape

The OSGIMF mimics the IGIMF but shows additional features. It differs from the IGIMF because the optimally-sampled result is a discrete function under binning. If all the clusters in the model had the same mass, optimal sampling would generate the same list of stars for all these clusters. This leads to gaps between the sampled stellar masses and peaks at the sampled masses.

In reality, clusters with different masses can smoothen this effect. With the currently used ECMF (Axiom 4 in Sect. 2.1), there exists a large percentage of clusters with mass $M_{\rm ecl} \approx 5$ or 6 $M_\odot$. The serrated features are the legacy of these clusters. Only when the ECMF slope $\beta < 2.1$, can there be enough high mass clusters, which all have different masses, to smoothen out the serrated feature. If a smoothly varying probability distribution of cluster masses is assumed at the mass boundaries rather than the sharp-edged ECMF in Eq. (9), there would also be no serrated features.

The above discussion only applies to the perfect deterministic scenario. Although astrophysical nature shows evidence to be closer to deterministic, i.e., a high level of self-regulation, it still possesses some level of randomness due to additional parameters not known to the theory. For instance, the angular momenta of clouds when star clusters form are not likely to be the same. This can result in a different stellar list for the embedded star clusters with the same mass and smoothen the final result.

For the present purpose, here we point out that if nature is somewhere close to the optimal sampling of stellar masses, there will be physical consequences. In particular the SFRs, stellar-mass buildup times and gas-depletion timescales of galaxies are affected significantly (Pflamm-Altenburg et al. 2007; Pflamm-Altenburg & Kroupa 2008, 2009). Different sampling methods with the same cluster scale IMF actually lead to different physical results. If the serrated feature is detected, it will strongly support optimal sampling and give direct information on the ECMF.

6. Conclusions

We have updated the $m_{\rm str,max}$–$M_{\rm ecl}$ and $M_{\rm ecl,max}$–SFR relation with newest observations. A comparison of the optimal sampling and random sampling predictions indicates that the optimal sampling scenario is favored.

The $\alpha_3^{\rm gal}$–SFR relation as a natural outcome of the IGIMF theory is also updated. It agrees with the observationally suggested trend.

For the first time, optimal sampling is introduced in the context of the IGIMF theory to generate a list of definite masses of stars in a galaxy. As a side effect, this also makes the sampling of stellar masses in a very massive galaxy computationally efficient[15].

We test and apply the improved optimal sampling and normalization method to further constrain the IGIMF theory. A prediction of the IGIMF model as defined by the axioms adopted here is that dwarf galaxies with $SFR < 10^{-4}\ M_\odot$/yr should host no SNII events in the absence of binary stars.

The OSGIMF largely agrees with previous IGIMF studies and shows a special serrated structure that previous integration calculations did not contain. This structure, if it exists, would be strong evidence for a deterministic and self-regulated star formation process.

[15] Unlike random sampling, optimal sampling follows a deterministic equation, giving a quick method to calculate the number of stars in a given mass range without sampling each star one by one.

Finally, we provide the publicly available Python computer module GalIMF for general use.

References

Andrews, J. E., Calzetti, D., Chandar, R., et al. 2013, ApJ, 767, 51
Baldry, I. K., & Glazebrook, K. 2003, ApJ, 593, 258
Banerjee, S., & Kroupa, P. 2015, ArXiv e-prints [arXiv:1512.03074]
Banerjee, S., Kroupa, P., & Oh, S. 2012a, ApJ, 746, 15
Banerjee, S., Kroupa, P., & Oh, S. 2012b, MNRAS, 426, 1416
Bastian, N., Covey, K. R., & Meyer, M. R. 2010, ARA&A, 48, 339
Bruzzese, S. M., Meurer, G. R., Lagos, C. D. P., et al. 2015, MNRAS, 447, 618
Chabrier, G. 2003, PASP, 115, 763
Chomiuk, L., & Povich, M. S. 2011, AJ, 142, 197
Dabringhausen, J., Hilker, M., & Kroupa, P. 2008, MNRAS, 386, 864
Dabringhausen, J., Kroupa, P., & Baumgardt, H. 2009, MNRAS, 394, 1529
Dabringhausen, J., Kroupa, P., Pflamm-Altenburg, J., & Mieske, S. 2012, ApJ, 747, 72
da Silva, R. L., Fumagalli, M., & Krumholz, M. 2012, ApJ, 745, 145
Dib, S., Kim, J., & Shadmehri, M. 2007, MNRAS, 381, L40
Dib, S., Schmeja, S., & Hony, S. 2017, MNRAS, 464, 1738
Disney, M. J., Romano, J. D., Garcia-Appadoo, D. A., et al. 2008, Nature, 455, 1082
Egusa, F., Sofue, Y., & Nakanishi, H. 2004, PASJ, 56, L45
Egusa, F., Kohno, K., Sofue, Y., Nakanishi, H., & Komugi, S. 2009, ApJ, 697, 1870
Elmegreen, B. G., & Scalo, J. 2006, ApJ, 636, 149
Elmegreen, B. G., & Shadmehri, M. 2003, MNRAS, 338, 817
Figer, D. F. 2005, Nature, 434, 192
Fontanot, F., De Lucia, G., Hirschmann, M., et al. 2017, MNRAS, 464, 3812
Fukui, Y., & Kawamura, A. 2010, ARA&A, 48, 547
Fumagalli, M., da Silva, R. L., & Krumholz, M. R. 2011, ApJ, 741, L26
Gargiulo, I. D., Cora, S. A., Padilla, N. D., et al. 2015, MNRAS, 446, 3820
Gunawardhana, M. L. P., Hopkins, A. M., Sharp, R. G., et al. 2011, MNRAS, 415, 1647
Gvaramadze, V. V., Weidner, C., Kroupa, P., & Pflamm-Altenburg, J. 2012, MNRAS, 424, 3037
Haghi, H., Khalaj, P., Hasani Zonoozi, A., & Kroupa, P. 2017, ApJ, 839, 60
Hasselquist, S., Shetrone, M., Smith, V., et al. 2017, ApJ, 845, 162
Hopkins, P. F. 2013, MNRAS, 433, 170
Hoversten, E. A., & Glazebrook, K. 2008, ApJ, 675, 163
Hsu, W.-H., Hartmann, L., Allen, L., et al. 2012, ApJ, 752, 59
Hsu, W.-H., Hartmann, L., Allen, L., et al. 2013, ApJ, 764, 114
Kennicutt, Jr., R. C. 1983, ApJ, 272, 54
Kennicutt, Jr., R. C., Tamblyn, P., & Congdon, C. E. 1994, ApJ, 435, 22
Kirk, H., & Myers, P. C. 2011, ApJ, 727, 64
Kirk, H., & Myers, P. C. 2012, ApJ, 745, 131
Koen, C. 2006, MNRAS, 365, 590
Kroupa, P. 1995a, MNRAS, 277, 1491
Kroupa, P. 1995b, MNRAS, 277, 1507
Kroupa, P. 2001, MNRAS, 322, 231
Kroupa, P. 2002, Science, 295, 82
Kroupa, P. 2005, in The Three-Dimensional Universe with Gaia, eds. C. Turon, K. S. O'Flaherty, & M. A. C. Perryman, ESA SP, 576, 629
Kroupa, P. 2015, Can. J. Phys., 93, 169
Kroupa, P., & Bouvier, J. 2003, MNRAS, 346, 343
Kroupa, P., & Weidner, C. 2003, ApJ, 598, 1076
Kroupa, P., Weidner, C., Pflamm-Altenburg, J., et al. 2013, in The Stellar and Sub-Stellar Initial Mass Function of Simple and Composite Populations, eds. T. D. Oswalt, & G. Gilmore, 115
Lada, C. J., & Lada, E. A. 2003, ARA&A, 41, 57
Lee, J. C., Gil de Paz, A., Tremonti, C., et al. 2009, ApJ, 706, 599
Leisawitz, D. 1989, BAAS, 21, 1189
Lieberz, P., & Kroupa, P. 2017, MNRAS, 465, 3775
Maíz Apellániz, J., Walborn, N. R., Morrell, N. I., Niemela, V. S., & Nelan, E. P. 2007, ApJ, 660, 1480
Marks, M., & Kroupa, P. 2012, A&A, 543, A8
Marks, M., Kroupa, P., Dabringhausen, J., & Pawlowski, M. S. 2012, MNRAS, 422, 2246
Matteucci, F., & Brocato, E. 1990, ApJ, 365, 539
Megeath, S. T., Gutermuth, R., Muzerolle, J., et al. 2016, AJ, 151, 5
Meidt, S. E., Hughes, A., Dobbs, C. L., et al. 2015, ApJ, 806, 72
Meurer, G. R., Wong, O. I., Kim, J. H., et al. 2009, ApJ, 695, 765
Oey, M. S., & Clarke, C. J. 2005, ApJ, 620, L43
Oh, S., & Kroupa, P. 2012, MNRAS, 424, 65
Peacock, M. B., Zepf, S. E., Kundu, A., et al. 2017, ApJ, 841, 28
Pflamm-Altenburg, J., & Kroupa, P. 2008, Nature, 455, 641
Pflamm-Altenburg, J., & Kroupa, P. 2009, ApJ, 706, 516
Pflamm-Altenburg, J., & Kroupa, P. 2010, MNRAS, 404, 1564
Pflamm-Altenburg, J., Weidner, C., & Kroupa, P. 2007, ApJ, 671, 1550
Pflamm-Altenburg, J., Weidner, C., & Kroupa, P. 2009, MNRAS, 395, 394
Pflamm-Altenburg, J., González-López lira, R. A., & Kroupa, P. 2013, MNRAS, 435, 2604
Ramírez Alegría, S., Borissova, J., Chené, A.-N., et al. 2016, A&A, 588, A40
Randriamanakoto, Z., Escala, A., Väisänen, P., et al. 2013, ApJ, 775, L38
Recchi, S., & Kroupa, P. 2015, MNRAS, 446, 4168
Renaud, F., Famaey, B., & Kroupa, P. 2016, MNRAS, 463, 3637
Robitaille, T. P., & Whitney, B. A. 2010, ApJ, 710, L11
Rybizki, J., & Just, A. 2015, MNRAS, 447, 3880
Salpeter, E. E. 1955, ApJ, 121, 161
Scalo, J. M. 1986, in Luminous Stars and Associations in Galaxies, eds. C. W. H. De Loore, A. J. Willis, & P. Laskarides, IAU Symp., 116, 451
Schulz, C., Pflamm-Altenburg, J., & Kroupa, P. 2015, A&A, 582, A93
Seigar, M. S., & James, P. A. 2002, MNRAS, 337, 1113
Shadmehri, M. 2004, MNRAS, 354, 375
Stephens, I. W., Gouliermis, D., Looney, L. W., et al. 2017, ApJ, 834, 94
Telford, O. G., Dalcanton, J. J., Skillman, E. D., & Conroy, C. 2016, ApJ, 827, 35
Thies, I., Pflamm-Altenburg, J., Kroupa, P., & Marks, M. 2015, ApJ, 800, 72
Tsujimoto, T. 2011, ApJ, 736, 113
Vazdekis, A., Cenarro, A. J., Gorgas, J., Cardiel, N., & Peletier, R. F. 2003, MNRAS, 340, 1317
Weidner, C., & Kroupa, P. 2004, MNRAS, 348, 187
Weidner, C., & Kroupa, P. 2005, ApJ, 625, 754
Weidner, C., & Kroupa, P. 2006, MNRAS, 365, 1333
Weidner, C., Kroupa, P., & Larsen, S. S. 2004, MNRAS, 350, 1503
Weidner, C., Bonnell, I. A., & Zinnecker, H. 2010, ApJ, 724, 1503
Weidner, C., Kroupa, P., & Pflamm-Altenburg, J. 2013a, MNRAS, 434, 84
Weidner, C., Kroupa, P., Pflamm-Altenburg, J., & Vazdekis, A. 2013b, MNRAS, 436, 3309
Weidner, C., Kroupa, P., & Pflamm-Altenburg, J. 2014, MNRAS, 441, 3348
Zapartas, E., de Mink, S. E., Izzard, R. G., et al. 2017, A&A, 601, A29
Zonoozi, A. H., Haghi, H., & Kroupa, P. 2016, ApJ, 826, 89

Appendix A: Disagreements about the $m_{\rm str,max}$–$M_{\rm ecl}$ relation

Some studies have been argued against the existence of a $m_{\rm str,max}$–$M_{\rm ecl}$ relation and favor the stochastic star formation scenario. Such claims are partially based on unresolved observations with large uncertainties on cluster age and mass determinations. More importantly, a typical issue many papers have, for instance in Fumagalli et al. (2011), Andrews et al. (2013), and Dib et al. (2017), is that these authors consider the $m_{\rm str,max}$–$M_{\rm ecl}$ relation as a simple truncation mass in a randomly sampled IMF (or ECMF)[16]. Although it has been stated clearly in Weidner et al. (2014) that this is not the case, neither Weidner & Kroupa (2006) nor the original IGIMF paper (Kroupa & Weidner 2003) highlighted the idea of optimal sampling, which was developed later (Kroupa et al. 2013). And the implementation of optimal sampling is mathematically more involved than drawing random numbers. Since this issue is still highly debated, we explain it again here.

The significant $m_{\rm str,max}$–$M_{\rm ecl}$ relation refers to the small scatter of the observational data, suggesting that one should apply a more deterministic sampling method such as optimal sampling, which results in a deterministic list of masses of the sampled stars. Given an embedded cluster mass, $M_{\rm ecl}$, the optimal sampling constraint (Eq. (4)) leads to a most massive star mass, $m_{\rm str,max}$, which automatically fulfills the empirical $m_{\rm str,max}$–$M_{\rm ecl}$ relation. This is different from a combination of truncation mass limit and random sampling. For example, in our Fig. 1 the optimally sampled result (the thick black line) reproduces the $m_{\rm str,max}$–$M_{\rm ecl}$ relation and describes the observational data rather than being an upper bound. The scatter around our theoretical prediction is accounted for by large observational uncertainties, systematic uncertainties, and small randomness due to additional parameters not known to the theory. If the $m_{\rm str,max}$–$M_{\rm ecl}$ relation is used as a truncation mass limit in cooperation with random sampling, all the sampled stars would be situated below the thick black line in Fig. 1, thus deviating from the observational data. So the counter-papers arguing against the $m_{\rm str,max}$–$M_{\rm ecl}$ relation actually disagree with the truncation-plus-random-sampling scenario, which is not what Weidner & Kroupa (2006) and Kroupa & Weidner (2003) implied[17] as has been already explained by Weidner et al. (2014).

Appendix B: The integrated galaxy-wide IMF for different assumptions

We show IGIMFs in Fig. B.1 for different SFRs and metallicities according to Eq. (8), where the metallicity of the gas phase of a galaxy is taking into consideration. Lower metallicity cases result in a more top-heavy IMF, but this metallicity dependence vanishes at low SFRs as the change in α_3 has no effect if there are no massive stars.

Six IGIMF models for different assumptions on α_3 and β are shown in Figs. B.2 to B.6. In the plot captions, "fixed α_3" means $\alpha_3 = 2.3$, "changeable α_3" means α_3 follows Eq. (5), "fixed β" means $\beta = 2$, "changeable β" means β follows Eq. (10), "Weidner β" means Eq. (10) is only applied when $SFR > 1\ M_\odot$/yr.

[16] As stated in the SLUG paper, see da Silva et al. (2012, their Appendix A), and Dib et al. (2017, their Sect. 5.2).

[17] The word "truncation" did not appear in Weidner & Kroupa (2006) and Kroupa & Weidner (2003). It only appears in Schulz et al. (2015) to describe the upper integration limit as mentioned above in Sect. 2.2.

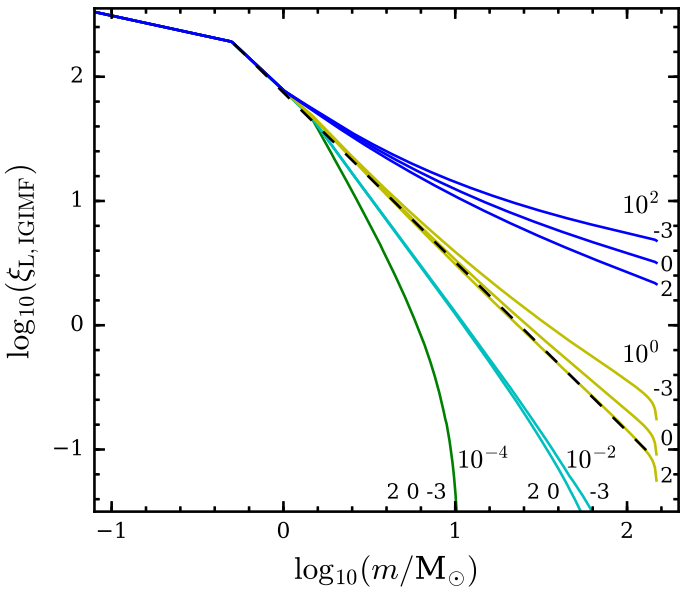

Fig. B.1. Same as Fig. 3 but using Eq. (8), with green, cyan, yellow, and blue lines for $SFR = 10^{-4}$, 10^{-2}, 10^0, and $10^2\ M_\odot$/yr, respectively. There are three cases for each color with [Fe/H] = –3, 0, and 2 from upper to lower lines labeled in the plot, however, the three green lines overlap and the lower two cyan lines also overlap.

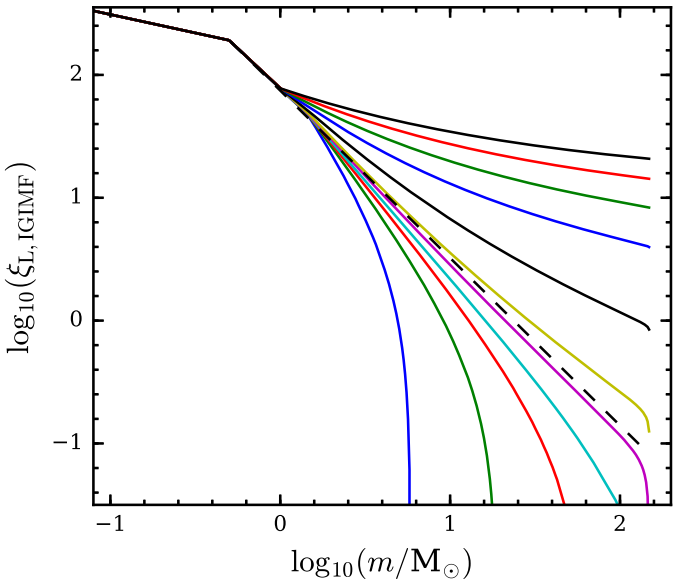

Fig. B.2. Same as Fig. 3 with changeable α_3 and Weidner β.

The "changeable α_3" and "changeable β" case plotted in Fig. 3 is our fiducial model for which the resulting $\alpha_3^{\rm gal}$–SFR relation best reproduces the observational constrains as shown in Fig. 6. Other models are shown below.

Appendix C: The $m_{\rm str,max}$–$M_{\rm ecl}$ relation and the OSGIMF for a constant α_3 assumption

If we assume $\alpha_3 = 2.3$ is a constant instead of varying according to Eq. (8) and keep everything else the same as Sect. 2.1, the resulting $m_{\rm str,max}$–$M_{\rm ecl}$ relation would have no steepening feature in Fig. 1, as shown in Fig. C.1. This change also removes the spoon feature in our Fig. 4, as shown in Fig. C.2.

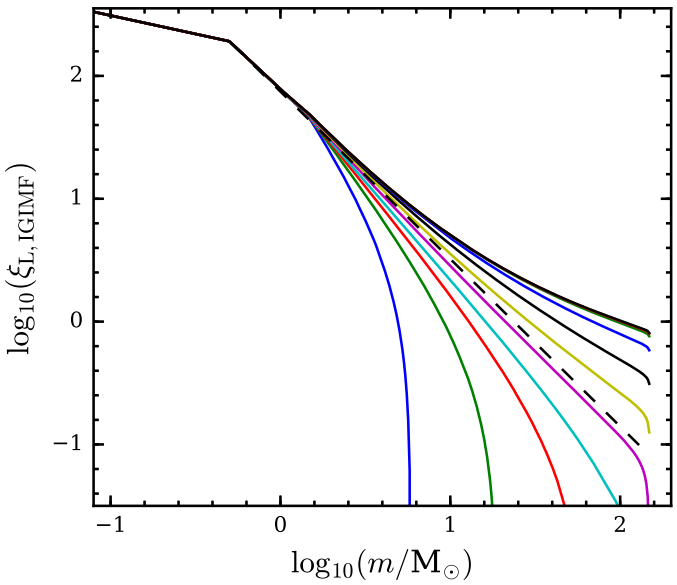

Fig. B.3. Same as Fig. 3 with changeable α_3 and fixed β.

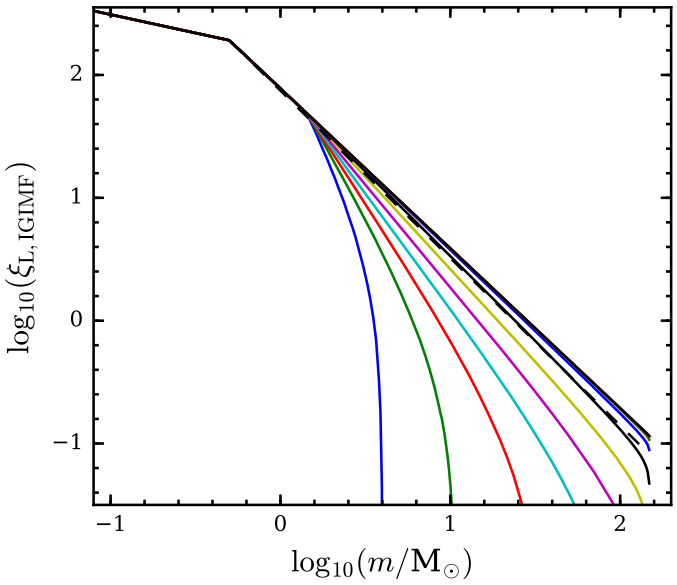

Fig. B.4. Same as Fig. 3 with fixed α_3 and changeable β.

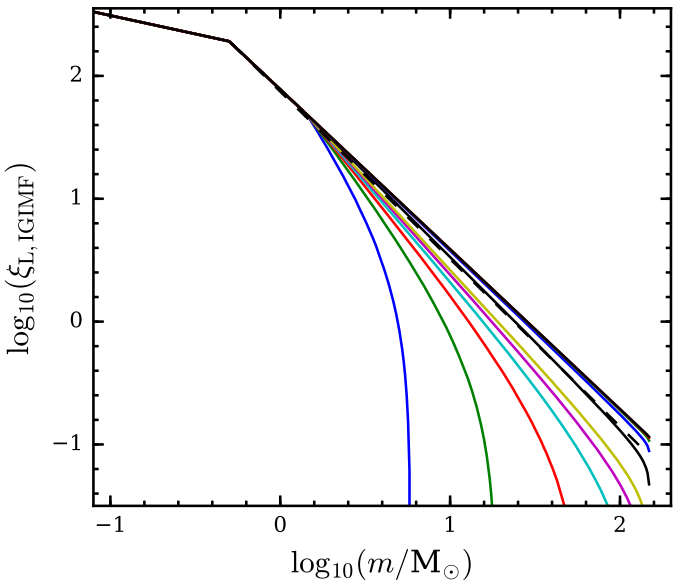

Fig. B.5. Same as Fig. 3 with fixed α_3 and Weidner β.

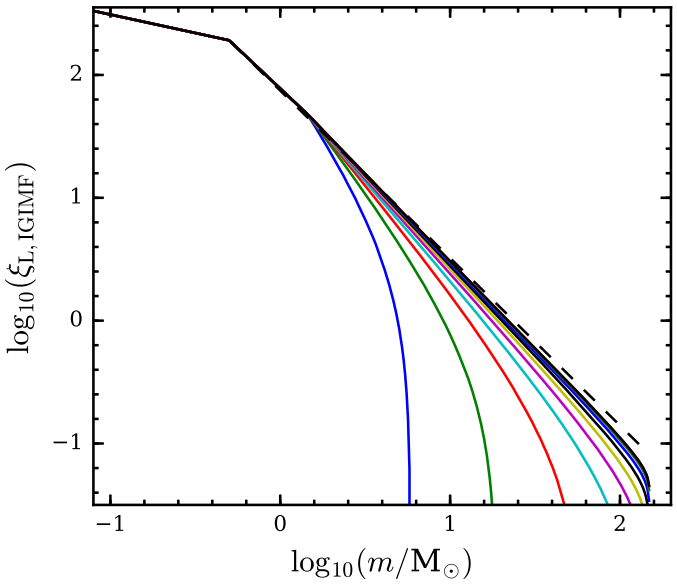

Fig. B.6. Same as Fig. 3 with fixed α_3 and fixed β.

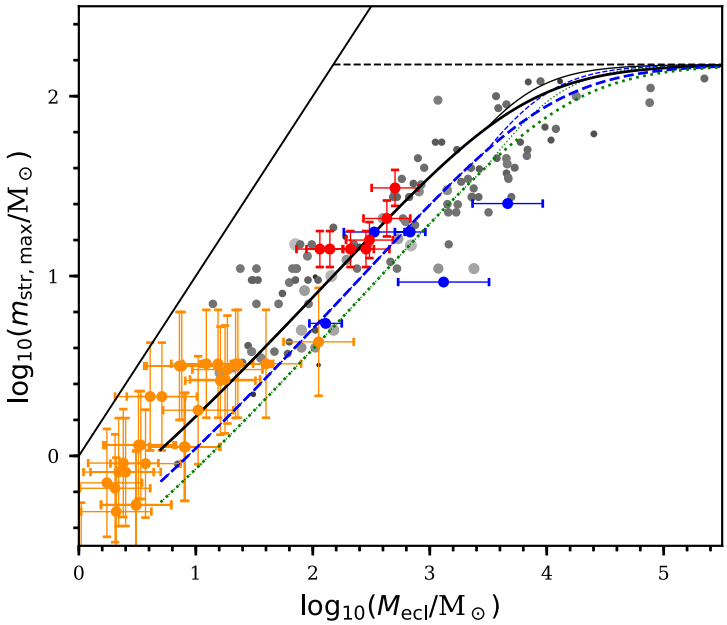

Fig. C.1. Same as Fig. 1 but with the thick lines applying the fixed IMF assumption of $\alpha_3 = 2.3$, while the thin lines indicate the line positions of Fig. 1.

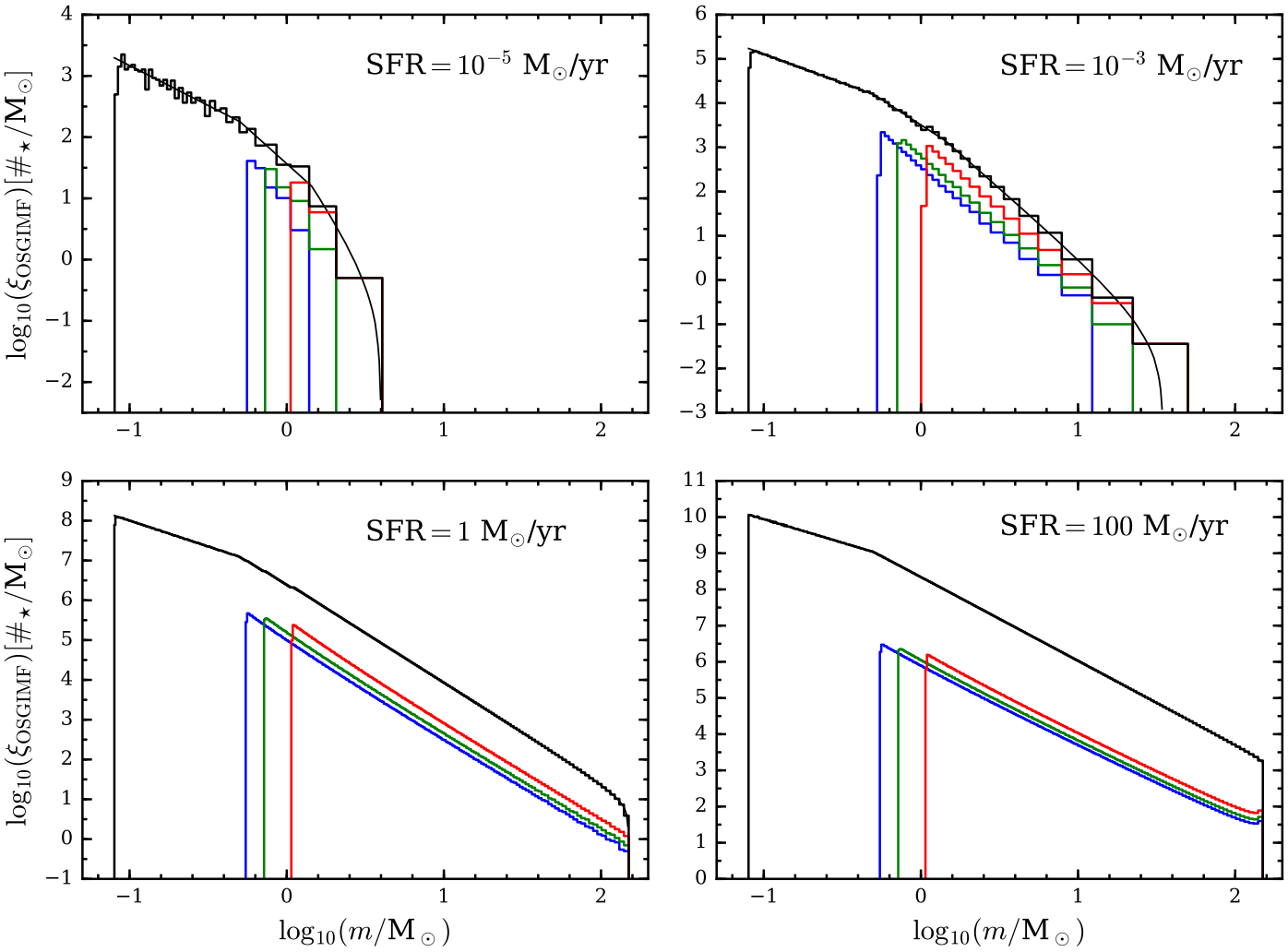

Fig. C.2. Same as Fig. 4 but with a fixed IMF assumption of $\alpha_3 = 2.3$. The spoon feature in the lower panels of Fig. 4 disappears here.